Open Access

Recent Progress in Science and Engineering

LIDSEN Publishing Inc.

Original Research

Boron-Based Solid Cooling Powder for Suppression of Lithium-Ion Battery Fires

Kadir Aydın [1,*], Çağrı Ün [2]

1. Department of Mechanical Engineering, OSTİM Technical University, Ankara, Türkiye; E-Mail: kadir.aydin@ostimteknik.edu.tr
2. Disaster Affairs and Risk Management Department, Adana Metropolitan Municipality, Adana, Türkiye; E-Mail: cagri.un@adana.bel.tr

* **Correspondence:** Kadir Aydın; E-Mail: kadir.aydin@ostimteknik.edu.tr

Academic Editor: Rajesh Kumar Raju

Special Issue: Reliability, Fault Diagnosis and Prognostics for Electric Vehicles and Energy Storage Systems

Recent Prog Sci Eng
2026, volume 2, issue 3
doi:10.21926/rpse.2603013

Received: May 11, 2026
Accepted: June 15, 2026
Published: July 01, 2026

Abstract

Thermal runaway in lithium-ion batteries (LIBs) is an escalating fire-safety problem in electric vehicles and battery energy-storage systems (BESS), and conventional water-based suppression has repeatedly been shown to delay propagation without preventing pack destruction or re-ignition. Solid, electrically non-conductive cooling agents are a promising but under-characterized alternative. This study addresses the absence of comparative, in-pack data on boron-based salt-hydrate cooling powders. Eight propane-burner ignition tests were performed on five LIB cell formats (NMC pouch, NMC pouch pack, LTO prismatic, NCA cylindrical and $LiFePO_4$ cylindrical) using manual water and Cobra-type extinguishers. As a separate proof-of-concept experiment, a 15-cell 18650 NMC pack (≈110 Wh) was fully immersed in solid borax-pentahydrate ($Na_2B_4O_7{\cdot}5H_2O$) cooling powder and exposed to a 1.4 kW external heat source for 23 min, with continuous K-type thermocouple logging. Water-based methods produced re-ignition and explosive cell ejection in cylindrical packs (peak 600-890°C; extinction times up to 9 min). The boron-immersed pack remained below 75°C for the

full 23-min exposure with a single transient 102.5°C reading that was an artifact of thermocouple withdrawal and showed no flame, gas venting or cell rupture. The behavior is interpreted through the endothermic dehydration cascade of borax pentahydrate (≈210 kJ/mol at 160-450°C) and a re-cast Arrhenius-type one-step thermal-runaway model. Within the explicit limitations of a single, uncontrolled comparison, boron-based salt-hydrate cooling shows strong potential as a non-toxic, non-carcinogenic, infrastructure-light, in-pack suppression strategy that is complementary to rather than a replacement for water-based methods. Controlled, replicated and scaled-up testing, together with material-level characterization, is identified as essential future work.

Keywords
Lithium-ion battery; thermal runaway; fire suppression; boron pentahydrate; borax; Arrhenius model; electric vehicle safety

1. Introduction

Lithium-ion batteries (LIBs) have become the dominant electrochemical-storage technology of the early 21st century. Global sales of electric-vehicle (EV) batteries alone are projected to exceed USD 3 billion per year by 2030, with ancillary growth in stationary battery energy storage systems (BESS) for renewable grid integration and industrial backup power [1, 2]. Of the six major commercial cathode chemistries [lithium cobalt oxide (LCO), lithium iron phosphate (LFP), lithium manganese oxide (LMO), nickel-cobalt-aluminum (NCA), nickel-manganese-cobalt (NMC) and lithium titanate (LTO)] the high-energy-density NMC and NCA formulations have been favored for passenger EV traction batteries (specific energy 220 and 280 Wh/kg respectively), while LFP, with a lower specific energy of approximately 140 Wh/kg, has gained ground in entry-level and Chinese-market BEVs as well as in BESS, owing to its higher thermal stability [3, 4].

The rise in deployment has been accompanied by a parallel rise in safety incidents. Thermal runaway [a self-accelerating sequence of exothermic decomposition reactions that begins when one or more cells exceed a chemistry-specific onset temperature (≈150°C for LCO, 180°C for NCA, 200°C for NMC, 250°C for LMO and LTO, 270°C for LFP)] is the principal failure mode [5, 6]. Once initiated, thermal runaway in an NMC-811 cell can propagate through a battery module in less than two minutes, releasing peak temperatures of 800-890°C, generating up to 25 L of combustible gases per Wh of stored energy, and producing toxic emissions including hydrogen fluoride, carbon monoxide and hydrogen [7, 8]. Real-driving fire incidents reported in 2024 confirm that conventional manual or automatic water suppression rarely fully extinguishes such fires before destruction of the pack, and that re-ignition events occurring 10-30 minutes after apparent extinction are common [9, 10]. The development of effective fire-suppression agents specific to LIB fires is therefore a high-priority research area in vehicle and stationary safety engineering.

This paper reports the results of an experimental campaign conducted jointly by Çukurova University, the University of Poitiers/National School of Mechanics and Aerotechnics (ISAE-ENSMA), the Pprime Institute, and the Departmental Fire and Rescue Service of the Vienne Region, in which five distinct cell formats and two extinguishing strategies (manual water and Cobra-type

extinguishers; solid boron-based powder) were tested. Building on the authors' earlier 2021 publication in Vehicles [11], the present article integrates the experimental observations with the most recent (2024-2025) thermal-runaway suppression literature, develops an Arrhenius-type one-step model relating measured pack temperatures to chemistry-specific activation energies, and provides a comparative quantitative analysis of solid-boron-powder cooling against the water mist, encapsulated-water-mist, and ammonium-bicarbonate carbonate-agent methods that have been characterized in the recent BESS suppression literature [12-14]. The boron-based approach is particularly well suited to Türkiye, which holds approximately 73% of world boron reserves [15] and where the development of value-added boron products is a strategic national priority.

To establish the gap addressed by this study, the remainder of this Introduction consolidates the relevant state of the art rather than treating it as a separate section. It reviews the thermal-runaway behavior of the principal LIB chemistries and cell formats (Sections 1.1-1.3), the main classes of fire-extinguishing agent and the specific limitations of water on LIB fires (Section 1.4), prior work on hydrated-salt and boron-based cooling agents (Section 1.5), and the one-step Arrhenius framework used to interpret the measurements (Section 1.6).

1.1 Lithium-Ion Cell Chemistries and Thermal-Runaway Thresholds

Six commercial LIB cathode chemistries account for the majority of the present-day market. Their thermal-runaway onset temperatures and specific energy densities are summarized in Figure 1 and Table 1. The data reflect a fundamental trade-off: cathode chemistries that maximize specific energy (NCA at 280 Wh/kg, NMC at 220 Wh/kg) operate close to the limit of cobalt-oxygen bond stability and undergo cathode oxygen release at 150-210°C, while olivine-structured LFP retains its phosphorus-oxygen framework up to 500-800°C [3, 16]. The LFP onset of thermal runaway is correspondingly the highest of the six chemistries (270°C); LFP fires also burn cooler (peak cell-face temperature ≈620°C) than NMC fires (≈800°C) and eject only 20-25% of the cell mass against 40-50% for NMC [4, 16].

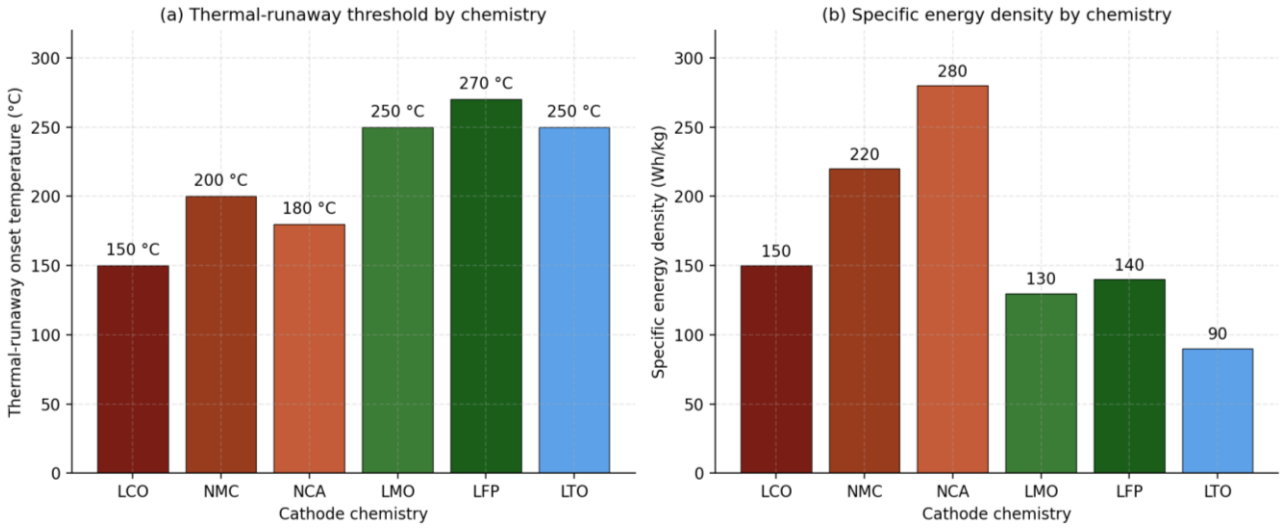

Figure 1 (a) Thermal-runaway onset temperature and (b) specific energy density of the six commercial LIB cathode chemistries [3, 4, 16].

Table 1 Thermal-runaway onset temperatures, specific energy densities and principal applications of the six commercial LIB cathode chemistries.

Chemistry	Cathode formula	TR onset (°C)	Energy density (Wh/kg)	Principal applications
LCO	$LiCoO_2$	150	150	Consumer electronics
NMC	$LiNiMnCoO_2$	200	150-220	Passenger EV traction
NCA	$LiNiCoAlO_2$	180	>280	Premium EV traction (Tesla)
LMO	$LiMn_2O_4$	250	100-130	Power tools, hybrid vehicles
LFP	$LiFePO_4$	270	90-160	Entry-level EV, BESS, buses
LTO	$Li_4Ti_5O_{12}$	250	60-110	Fast-charge buses, transit

1.2 Mechanism of Thermal Runaway

Thermal runaway in LIBs is a three-stage cascade of exothermic decomposition reactions that release the chemical and electrochemical energy stored in the cell as heat (Figure 2). In stage 1, an abuse condition like internal short circuit, mechanical penetration, overcharging, or external heating raises the cell temperature above the onset value of the solid-electrolyte-interphase (SEI) film, typically 80-120°C. The SEI decomposes and exposes the lithiated graphite anode (Li_xC_6) to the electrolyte, releasing additional heat. In stage 2, between roughly 130°C and 200°C, the polyolefin separator (polyethylene, polypropylene) melts and ruptures; the cathode and anode short internally, and the electrolyte solvents (ethylene carbonate, dimethyl carbonate, ethyl methyl carbonate) begin to volatilize and react. In stage 3, above the cathode decomposition temperature, the metal-oxide cathode releases lattice oxygen, which combines with the volatilized electrolyte and any released hydrogen and methane in a violent combustion event that may take the form of an open flame, a high-velocity jet, or, in confined cylindrical formats, a missile-effect explosion [5, 17, 18].

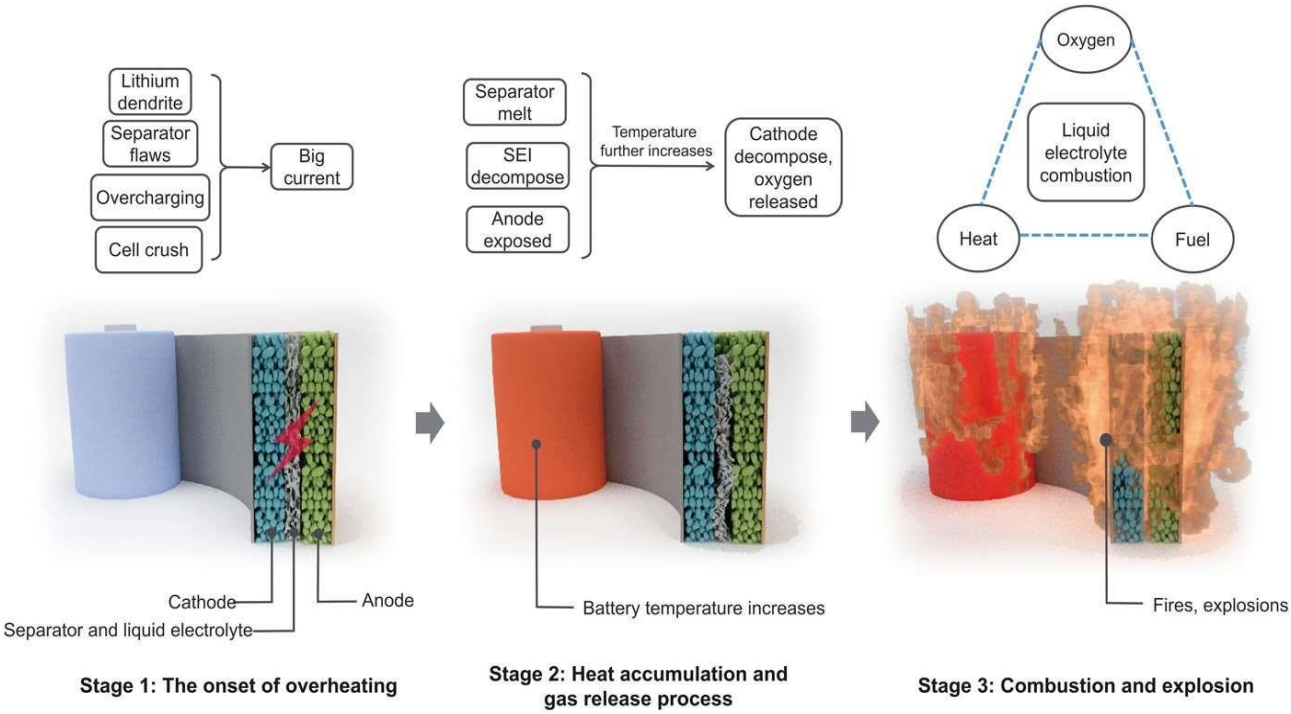

Figure 2 Three-stage representation of thermal runaway in a Li-ion cell [5].

1.3 Cell Formats and Cooling Considerations

Three commercial cell formats dominate automotive and stationary applications: cylindrical hard-case cells (typically 18650 or 21700 form factor), prismatic hard-case cells, and pouch cells with a flexible aluminum-laminate envelope (Figure 3). The format strongly influences the thermal-runaway propagation mechanism and the suitability of different suppression strategies. Cylindrical cells distribute internal pressure evenly across their circumference and are equipped with safety vents that release accumulated gas; thermal runaway in cylindrical cells is therefore typically characterized by jet venting and, in confined packs, by missile-like ejection of the cell can. Prismatic cells, particularly LTO formulations, are mechanically constrained and tend to extinguish more quickly than NMC pouch cells; however, they may undergo violent rupture if their casing is over pressurized. Pouch cells, with their high packaging efficiency (90-95% cell volume utilization) but low mechanical rigidity, propagate thermal runaway most rapidly due to their planar geometry and require active thermal management even in nominal operation [19, 20].

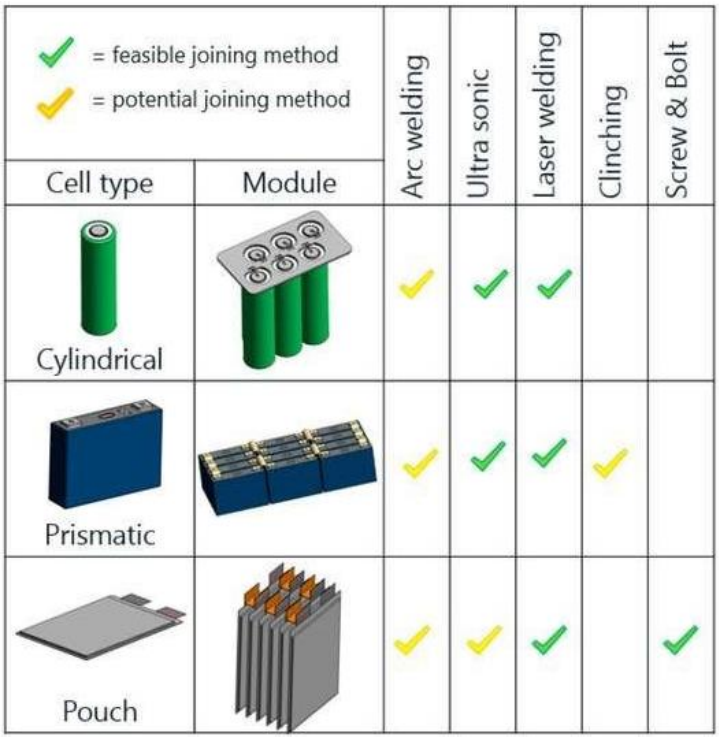

Figure 3 Schematic of the three commercial lithium-ion cell formats: cylindrical, prismatic, and pouch [19, 20].

Within each cell, four functional components (cathode, anode, electrolyte and separator) operate in concert (Figure 4). The cathode and anode set the cell capacity and voltage, while the electrolyte and separator set the safety margin. Damage to the separator is the most common direct precursor of thermal runaway: a 100 µm-scale defect in the polyolefin separator allows direct cathode-anode contact, generating a localized internal short circuit with current densities exceeding 100 A/cm^2 and sustained heat-release rates above 100 W/cell [21].

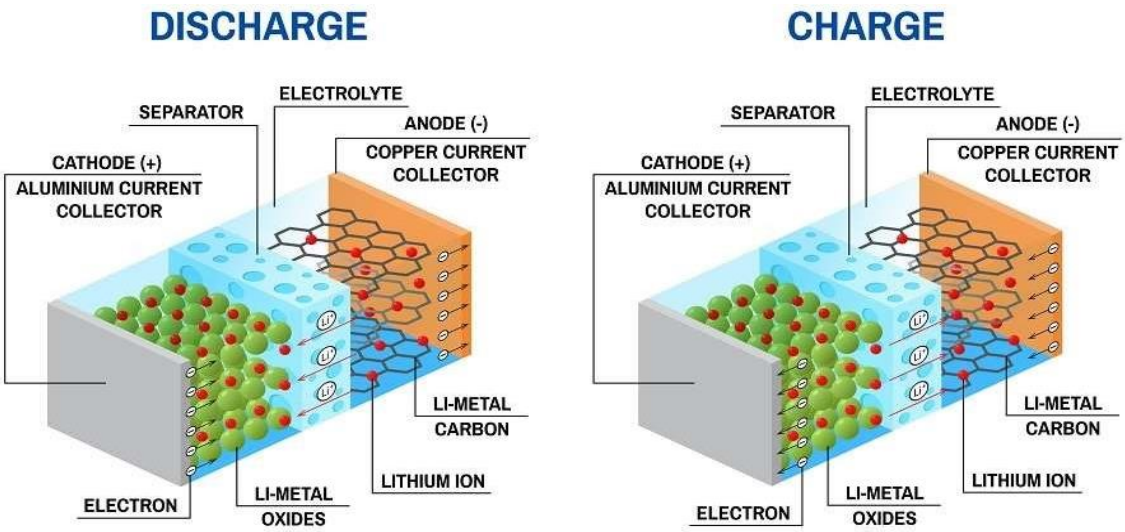

Figure 4 Schematic of charge and discharge in a Li-ion cell [21].

1.4 Conventional Suppression Strategies and Extinguishing Agent Classes

Three principles underpin all fire-suppression chemistry:

- cooling (removing heat from the burning material below its ignition temperature);
- oxygen displacement (interposing an inert atmosphere);
- chain-reaction interruption (chemically deactivating the radical species (OH, H, O) that propagate combustion).

Practical extinguishing agents combine these three principles to differing degrees, and a brief comparison frames why a solid salt hydrate is of interest for LIB fires. Water and water mist act chiefly by cooling and by latent-heat absorption during evaporation, but they conduct electricity and react with reactive metals (detailed below); carbon dioxide and inert gases act by oxygen displacement, giving clean, residue-free knock-down but negligible cooling and no re-ignition barrier - a decisive drawback for cells that release their own lattice oxygen; foams form a smothering, oxygen-excluding blanket with some cooling, but drain and collapse on hot, near-vertical cell surfaces; and conventional dry chemical powders (mono-ammonium phosphate, sodium bicarbonate) interrupt the radical chain reaction and smother the flame, yet deliver little sustained cooling and, for mono-ammonium phosphate, decompose into corrosive, toxic phosphorus and nitrogen oxides. Against this background a hydrated-salt solid powder is attractive because it couples the electrical safety and smothering action of a dry powder with a cooling capacity - supplied by endothermic dehydration - that approaches that of water (Section 1.5).

Conventional water-based extinguishers act predominantly through cooling: a liter of water absorbs approximately 313 kJ in heating from 25°C to 100°C, plus a further 2,300 kJ on completely vaporizing at 100°C, yielding a total cooling capacity of ≈2.6 MJ/L [22]. However, water suffers from three intrinsic limitations when applied to LIB fires:

- Reactivity with active metals. Lithiated graphite and exposed reactive metals (Al, Li, Cu) react exothermically with steam, generating hydrogen gas that further fuels combustion. The aluminum-water reaction generates 280 kJ/mol Al at temperatures above 600°C [22]:

$$2Al(s) + 6H_2O(g) \rightarrow 2Al(OH)_3 + 3H_2(g) \quad (1)$$

and the hydrogen so released combusts with atmospheric oxygen to regenerate water vapor, but only after passing through an explosive intermediate state:

$$2H_2(g) + O_2(g) \rightarrow 2H_2O(g) \quad (2)$$

- Electrical hazard. Pack voltages of 400-800 V remain present after thermal runaway is initiated, and water provides a direct conduction path between live components and ground.
- Limited accessibility. Pack-level water injections require either deformation of the pack housing or activation of fusible vents, both of which are not always present in current production EVs.

The water-based cooling capacity Q_{cool} for an applied mass mw of water at initial temperature T_0 heated to a final temperature T_f (with full vaporization) is given by the standard sensible-plus-latent expression:

$$Q_{cool} = m_w\left(c_p \Delta T + L_v\right) \quad (3)$$

where $\Delta T = T_f - T_0$, C_p is the specific heat capacity (4.18 kJ/kg·K for liquid water), and L_v is the latent heat of vaporization (2,260 kJ/kg at 100°C). Equation (3) sets the upper bound on the cooling that water can provide: even when fully consumed, 1 L of water cannot extract more than ≈2.6 MJ from a burning cell. A 60 kWh NMC pack contains approximately 216 MJ of stored chemical energy, of which an estimated 30-40% may be released during full thermal runaway. Even allowing for radiative and convective losses, the bare cooling capacity of water is therefore only marginally sufficient to absorb the heat of a single major thermal-runaway event in a typical EV pack [9, 10].

1.5 Hydrated-Salt and Boron-Based Cooling Agents: Prior Work

Hydrated (crystal-water-bearing) inorganic salts have emerged as a distinct class of LIB cooling and fire-suppression agents precisely because they combine a large endothermic capacity with electrical non-conductivity. Li et al. [23] systematically screened seven salt hydrates with different crystal-water contents as dry-powder extinguishants and showed, by differential scanning calorimetry, that the endothermic enthalpy released below 150°C can exceed 800 kJ/kg - sufficient to interrupt thermal-runaway propagation - while electric breakdown voltages of 4-60 kV confirm that, unlike liquid water, these powders do not provide a conduction path between live pack components. Borax pentahydrate ($Na_2B_4O_7{\cdot}5H_2O$), the active component of the present agent, belongs to exactly this family: it carries five molecules of crystal water that are released in a stepwise endothermic dehydration cascade (Section 2.2).

Several recent studies have exploited salt hydrates for battery protection in adjacent configurations. Lin et al. [24] integrated latent-heat and thermochemical storage in an inorganic salt hydrate that both delayed thermal runaway and inhibited cell-to-cell propagation, and composite phase-change materials built on $Na_2SO_4{\cdot}10H_2O$ and the alum-type hydrate $KAl(SO_4)_2{\cdot}12H_2O$ have reported latent heats near 227 J/g and thermal conductivities of ≈1.4 W/(m·K) when blended with expanded graphite [25]. These works, however, deploy the salt hydrate as an inter-cell barrier plate, an encapsulated phase-change composite, or an external spray, and most are evaluated on single cells or two-cell propagation pairs. The specific configuration examined here - a cylindrical 18650 pack fully immersed in loose boron-salt-hydrate powder so that every cell face is in direct conductive

contact with the agent - has not, to the authors' knowledge, been reported. It is this in-pack immersion geometry, rather than the salt-hydrate chemistry itself, that constitutes the novel contribution of the present study. It is acknowledged that the cited works provide the material-level characterization (DSC/TG enthalpies, conductivity) that the present proof-of-concept does not, a point returned to in Sections 2.4 and 4.4.

1.6 Thermal-Runaway Modelling Framework (Literature-Based Models)

1.6.1 One-Step Arrhenius Reaction-Rate Model

The cell-level temperature evolution during thermal runaway can be modeled, to first order, as the result of competition between an Arrhenius-type exothermic heat generation source and a heat-loss sink representing convection, radiation, and any imposed cooling. Following Hatchard et al. [26] and the recent refinements of Ruth et al. [27], the reaction-rate constant for the dominant decomposition reaction is written:

$$k(T) = A \exp\left(-\frac{E_a}{RT}\right) \tag{4}$$

where A is the pre-exponential factor (s^{-1}), E_a is the activation energy (kJ/mol), R = 8.314 J/(mol·K) is the universal gas constant, and T is the absolute temperature. The corresponding heat-generation rate per unit volume is then:

$$q_{gen} = \Delta H \cdot A \cdot c \cdot \exp\left(-\frac{E_a}{RT}\right) \tag{5}$$

where ΔH is the reaction enthalpy (kJ/mol of reactant) and c is the local concentration of unreacted material. For NMC-721 cathode chemistry, the most recent ARC-fitted parameters are $A = 2.1 \times 10^{10}$ s^{-1}, E_a = 130 kJ/mol and ΔH = 850 kJ/kg of active material [27, 28]. The reaction extends in three sequential stages (SEI decomposition, separator melt and cathode oxygen release), each with its own (A, E_a, ΔH) triplet.

1.6.2 Cell-Level Energy Balance

Treating the cell as a lumped thermal mass, the energy balance becomes:

$$\rho V c_p \frac{dT}{dt} = q_{gen} - q_{cool} - hA_s(T - T_{amb}) \tag{6}$$

where ρ is density, V is cell volume, c_p is specific heat, q_{gen} is the Arrhenius source of equation (5), q_{cool} is the rate of heat removal by an applied suppressant, h is the convective heat-transfer coefficient and A_s the cell surface area. Thermal runaway is initiated when $q_{gen} > q_{cool} + hA_s(T - T_{amb})$ and self-sustains until the reactant concentration c falls to zero. The dimensionless lithium concentration in the SEI layer x_{SEI} evolves according to:

$$\frac{dx_{SEI}}{dt} = -A_{SEI} \cdot x_{SEI} \cdot \exp\left(-\frac{E_{SEI}}{RT}\right) \tag{7}$$

with A_{SEI} = 1.7 × 10^{15} s^{-1} and E_{SEI} = 135 kJ/mol [26, 29]. The total exothermic heat release summed over all reactions is:

$$Q_{tot} = \Sigma_i \Delta H_i \cdot k_i(T) \cdot c_i \tag{8}$$

1.6.3 Critical Condition for Thermal Runaway and Time-To-Runaway

Combining equations (5) and (6), the critical temperature T_{cr} above which thermal runaway becomes unavoidable is defined by the condition:

$$q_{gen}(T_{cr}) = q_{cool}(T_{cr}) \tag{9}$$

Below T_{cr}, the cooling rate exceeds the heat-generation rate and any temperature excursion decays. Above T_{cr}, the heat-generation rate dominates, and the cell temperature accelerates exponentially. The time to reach thermal runaway from an initial temperature T_0 for an externally imposed heat input q_h can be approximated, following Wang et al. [30], as:

$$t_{TR} = \frac{E_a}{R{T_{TR}}^2} \cdot \frac{T_{TR} - T_0}{A \cdot q_h} \tag{10}$$

Equation (10) shows that t_{TR} is sensitive to (E_a, T_{TR}^2): a 30 K reduction in T_{TR} (i.e., moving from LFP at 270°C to NMC at 200°C) reduces t_{TR} by approximately a factor of three for the same external heat input. This explains the much greater fire-safety challenge posed by NMC and NCA chemistries relative to LFP and LTO.

1.6.4 Suppression Effectiveness Metric

A simple, dimensionless metric for the effectiveness of a given suppression strategy is the temperature-suppression ratio:

$$\eta_{sup} = 1 - \frac{T_{max,sup}}{T_{max,ref}} \tag{11}$$

where $T_{max,\ sup}$ is the peak temperature reached during the suppressed test and $T_{max,\ ref}$ is the peak temperature for an unsuppressed reference test of identical cell chemistry, format and ignition source. η_{sup} = 1 corresponds to perfect suppression (no temperature rise above ambient); η_{sup} = 0 corresponds to no suppression effect.

Aim and Scope. Against this state of the art, the present study pursues three objectives: (i) to document, on a common 400 kW propane-burner ignition platform, how water-based suppression performs across five representative LIB cell formats and chemistries, with particular attention to the re-ignition and missile-effect behavior of cylindrical packs; (ii) to demonstrate, as a proof of concept, whether full immersion of a cylindrical 18650 pack in a solid borax-pentahydrate cooling powder can hold the pack below its thermal-runaway onset under sustained external heating; and (iii) to interpret the observed behavior with the one-step Arrhenius framework of Section 1.6 and to position it quantitatively against recently reported water-mist, microcapsule and salt-hydrate methods. The study is deliberately framed as a first, single-configuration demonstration; the

controlled, replicated and material-level work required to turn it into a validated suppression solution is set out in Sections 2.4 and 4.4.

2. Materials and Methods

2.1 Cells, Modules and Ignition Source

Six cell formats from four chemistries (NMC, LTO, NCA, LFP) were tested. The principal characteristics are summarized in Table 2. Pouch cells (types 1, 2, 3) were of NMC chemistry, prismatic cells (type 4) were of LTO chemistry, and cylindrical cells were of NCA (type 5) and LFP (type 6) chemistries. All cells were tested in a fully charged state (state of charge 100%).

Table 2 Technical characteristics of the cells used in the experiments at the University of Poitiers/ISAE-ENSMA [11].

Cell type	Chemistry & format	Cells/module	Module mass (kg)	TR onset T (°C)
Type 1	NMC pouch	20	28	≈200
Type 2	NMC pouch (large pack)	176	280 ± 5	≈200
Type 3	NMC pouch (medium pack)	48	81-83	≈200
Type 4	LTO prismatic	276	260 ± 5	≈250
Type 5	NCA cylindrical, plastic	-	13 (scooter)	≈180
Type 6	LFP cylindrical, plastic	-	20 (leisure)	≈270

To ensure reproducibility, the following details apply to all tests. Every cell and pack was tested at 100% state of charge (SoC). Thermal runaway was forced by external heating only: a 400-kW propane gas burner positioned beneath the specimen, applied continuously until visible runaway initiated (typically 30-90 s after ignition); no nail penetration, overcharge, or mechanical abuse was used, so the heat source in Tests T1-T8 is external rather than internally generated. Two suppression tools were used: a manual low-pressure water lance for single cells, and a Cobra-type high-pressure water-with-additive lance, capable of perforating thin metallic enclosures, for packs. Cell-surface and flame temperatures were recorded by the host laboratory using K-type thermocouples and infrared instrumentation. The boron-cooling experiment (Test T9), described in Section 2.3, used a separate setup at Çukurova University and a single continuously logged in-pack K-type thermocouple. The two campaigns were conducted on different platforms and are therefore compared qualitatively rather than as a controlled head-to-head trial; this limitation is stated explicitly in Section 2.4 and revisited in Section 4.4.

Ignition was provided by a 400-kW propane gas burner placed beneath the cell or pack. Cells were heated until thermal runaway became visible (typically 30-90 s after ignition). For the eight water-suppression tests (Tests T1-T8), a manual extinguisher (low-pressure water lance) and, for cylindrical-cell packs, a Cobra-type extinguisher (high-pressure water-with-additive lance capable of penetrating thin metallic enclosures) were used. The full test matrix is given in Table 3.

Table 3 Test matrix of the eight University of Poitiers/ISAE-ENSMA experiments and the boron-cooling experiment performed at Çukurova University.

No.	Cell/module	Suppression	Objective
T1, T2	**Type 1, 2 (NMC pouch)**	None (heat exposure)	Document thermal-runaway temperature rise
T3	**Type 4 (LTO prismatic)**	Manual water	Effect of water on LTO prismatic
T4	**Type 1 (NMC pouch, Al/plastic pack)**	Cobra extinguisher	Pack-level water penetration
T5	**Type 3 (NMC pouch, steel pack)**	Cobra extinguisher	Steel-cased pack-level penetration
T6	**Type 2 (NMC pouch pack)**	Cobra extinguisher	Pack-level reactivity
T7	**Type 5 (NCA cylindrical)**	Cobra extinguisher	Real EV-scooter battery suppression
T8	**Type 6 (LFP cylindrical)**	Cobra extinguisher	LFP cylindrical pack suppression
T9	**15 × 18650 (NMC cylindrical)**	Solid boron powder cooling	Boron-pentahydrate-cooled pack heat-up

2.2 Boron-Based Solid Cooling Powder: Composition and Properties

The boron-based extinguishing chemical used in the present work is a B-C-class fire-extinguishing powder developed by Demircan Fire (commercial name Fireborex) [31]. Its principal active component is borax pentahydrate ($Na_2B_4O_7{\cdot}5H_2O$), with the composition reported in Table 4. Borax pentahydrate is obtained from the Eti Maden tincal mine (Türkiye), which holds 73% of the world's reserves of refined boron compounds [15, 32]. The substance is non-carcinogenic, has a longer shelf life than ammonium-phosphate-based dry chemical extinguishers, and forms a glassy film at temperatures above ≈600°C that suppresses re-ignition.

Table 4 Composition of the boron-based B-C-class fire-extinguishing chemical used in the cooling experiment [31].

Component	CAS number	Concentration (% w/w)
Borax pentahydrate ($Na_2B_4O_7{\cdot}5H_2O$)	12179-04-3	10-20
Silica (SiO_2)	112926-00-8	<1
Sodium bicarbonate ($NaHCO_3$)	144-55-8	15-30
Inert carriers, surfactants	-	Balance

On heating, borax pentahydrate undergoes a cascade of three endothermic dehydration steps:

$$Na_2B_4O_7 \cdot 5H_2O \rightarrow Na_2B_4O_7 \cdot 2H_2O + 3H_2O(g) \quad (12)$$

followed by the further loss of water to borax monohydrates at 290-299°C and to anhydrous borax at 400-450°C [31, 33]. Each step is endothermic, with an enthalpy of dehydration approximately equal to the latent heat of vaporization of the released water (≈42 kJ/mol H_2O at the relevant temperature). The total endothermic heat absorbed by a mass m_B of boron pentahydrate is:

$$Q_B = m_B \cdot \Sigma_j \left(n_j \cdot \Delta H_{v,j} \right) \tag{13}$$

where n_j is the number of moles of water released in step j and $\Delta H_{v,j}$ is the corresponding latent heat. With three dehydration steps releasing a total of 5 mol H_2O per mol $Na_2B_4O_7 \cdot 5H_2O$, the total endothermic capacity is approximately 210 kJ/mol of borax pentahydrate, distributed across the three thresholds shown in Figure 5.

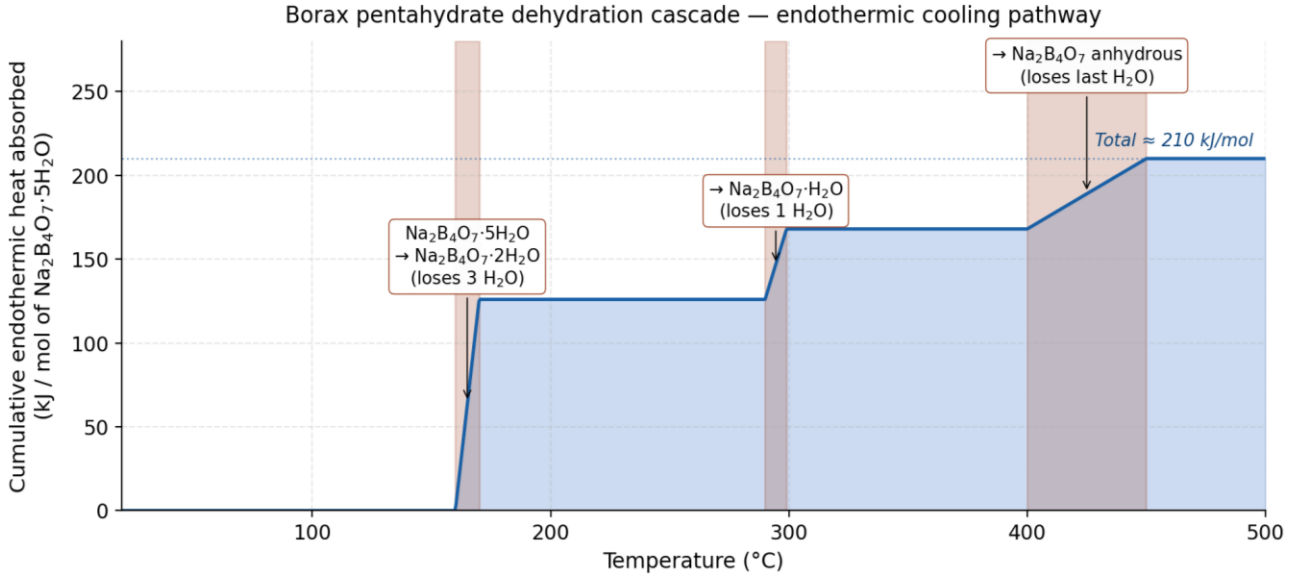

Figure 5 Cumulative endothermic heat absorbed by borax pentahydrate during its dehydration cascade.

2.3 Boron-Cooling Experimental Setup

Fifteen 18650-format cylindrical NMC cells (nominal capacity 2,000 mAh each, total stored energy ≈110 Wh) were connected in series by a thin steel wire and placed inside a steel box of internal volume 700 cm^3. The box was then filled with boron-based solid cooling powder until the cells were entirely covered, and the assembly was placed on top of a 1.4 kW resistive heating furnace (Figure 6). A K-type thermocouple was inserted into the center of the box, in direct contact with one of the cells. The full setup was operated continuously for 23 minutes; the heating furnace was switched on at t = 0, and the temperature was logged at 1 s intervals.

Figure 6 Boron-pentahydrate cooling experimental setup at Çukurova University.

2.4 Thermophysical Properties and Characterization Status of the Boron Powder

Thermophysical properties and barrier-formation mechanism. The cooling action of the powder rests on three thermophysical mechanisms, whose governing parameters are summarized here together with an explicit statement of which were measured and which were taken from the literature. (i) Endothermic dehydration: each of the three dehydration steps of borax pentahydrate releases crystal water with an enthalpy close to the latent heat of vaporization of water (≈42 kJ/mol H_2O), giving ≈210 kJ/mol of borax pentahydrate, i.e. ≈0.55 MJ/kg from dehydration alone; the step temperatures (160-170°C, 290-299°C, 400-450°C) and enthalpies are taken from the thermal-analysis study of Akbay and Altıokka [33], not measured here. For comparison, salt hydrates with higher crystal-water content can reach DSC endothermic enthalpies above 800 kJ/kg below 150°C [23], indicating clear room to optimize the agent. (ii) Sensible heat: with a specific heat capacity of the powder of order 1.0-1.4 kJ/(kg·K) for sodium-borate solids and a bulk density of ≈1.15 g/cm^3, the ≈800 g fill provides additional sensible storage; these values are nominal, drawn from material handbooks rather than measured on the present batch. (iii) Insulation: the granular packing has a low effective thermal conductivity (estimated 0.2-0.4 W/(m·K) for a porous sodium-borate powder bed), which limits radiative and conductive heat transfer from the heater to the cells.

Barrier formation. Above ≈600°C, the dehydrated residue (sodium borate/boron oxide) softens and forms a glassy, oxygen-excluding film over exposed surfaces, which is the mechanism proposed to suppress re-ignition. In the present work, this barrier is inferred from the observed absence of re-ignition and from the known glass-forming behavior of borate melts; it was not independently verified. We did not perform SEM, XRD, or TG-DSC on the post-test residue, and we did not measure thermal conductivity, specific heat, or phase-change kinetics on this specific powder. These measurements are necessary to confirm the barrier mechanism and to quantify the kinetics, and they are identified as priority future work in Section 4.4. The values quoted above should therefore

be read as literature- and handbook-based estimates that bound the expected behavior, not as characterized properties of the tested batch.

2.5 Ethics Statement

This study did not involve human participants, human-derived tissue, or animal subjects, and therefore no institutional ethical-review-board approval or informed-consent procedure was required. All experimental activities were conducted under controlled fire-laboratory conditions at the University of Poitiers/ISAE-ENSMA Pprime Institute (Poitiers, France) and at the Çukurova University Fire-Test Laboratory (Adana, Türkiye), in full compliance with the host institutions' standard operating procedures for high-voltage lithium-ion battery fire testing. Tests were performed in dedicated outdoor or naturally ventilated areas with the on-site presence and operational support of the Departmental Fire and Rescue Service of the Vienne Region (France) and the Departmental Fire and Rescue Service of the Adana Metropolitan Municipality (Türkiye). All test personnel wore certified personal protective equipment, including self-contained breathing apparatus where toxic gas release (HF, CO, hydrocarbons) was anticipated, and minimum exclusion radii were enforced to mitigate the risk of cell ejection (missile effect) and thermal-runaway propagation. Test residues, including burnt cell debris and electrolyte residues, were collected and disposed of as hazardous waste in accordance with EU Directive 2008/98/EC and the corresponding Turkish hazardous-waste regulations. The authors declare that the experimental data, figures, and temperature recordings reported in this paper are original, accurate, and have not been manipulated. The work has not been submitted, in whole or in part, for publication elsewhere.

3. Results

3.1 Water-Suppression Tests (Tests T1-T8)

Water-suppression tests were divided into single-cell heating tests (Tests T1-T3), pack-level Cobra-extinguisher tests on prismatic and pouch packs (Tests T4-T6), and Cobra-extinguisher tests on real cylindrical EV-scooter and leisure-vehicle batteries (Tests T7-T8). The principal experimental observations are summarized below.

Single-cell NMC pouch fires (Tests T1-T2, Figure 7) progressed rapidly. Once the surface temperature reached the manufacturer-quoted thermal-runaway onset of 200°C, the aluminum-laminate envelope ruptured, and the cell entered open-flame combustion within approximately 15 s. Flame temperatures of 600-800°C were observed; the entire cell was consumed within 90 s. By contrast, the LTO prismatic cell (Test T3, Figure 8) burned much more slowly: the cell case did not rupture during the test, and combustion was confined to electrolyte vapor leaking through the safety vent. Manual water extinguishing was effective on the LTO cell within 30 s, although a residual smolder persisted for several additional minutes.

Figure 7 Single-cell NMC pouch combustion (Tests T1-T2).

Figure 8 NMC pouch and LTO prismatic cells (Tests T1-T3).

Pack-level water-suppression tests on pouch packs (Tests T4-T5, Figure 9) demonstrated the importance of the casing material. The aluminum-and-plastic pack of Test T4 melted progressively, eventually allowing water from the Cobra extinguisher to reach the cells; the steel-cased pack of Test T5 required mechanical deformation or melting of fusible parts before water could be injected. The pouch-cell pack of Test T6 underwent a violent rupture as the molten aluminum of the cell case explosively combined with the released electrolyte. After approximately 9 minutes of total exposure, all three packs were eventually extinguished, although the residual cell debris continued to off-gas for several hours.

Figure 9 Pack-level NMC pouch and pack fires (Tests T4-T6).

The most challenging tests were the cylindrical-cell scooter and leisure-vehicle batteries (Tests T7-T8, Figure 10, Figure 11). Cylindrical cells, equipped with safety vents, repeatedly ejected gas and partial cell contents under the missile effect characteristic of pressurized-can rupture. The 2 kWh NCA scooter battery (Test T7) underwent the first thermal runaway at approximately 3 minutes of heating, was apparently extinguished, then re-ignited 4 minutes later in a second runaway accompanied by abundant white smoke and explosive cell ejections. The 20 kg LFP leisure-vehicle battery (Test T8) entered a sustained 9-minute combustion punctuated by repeated explosions, with cells launched several meters from the test bench (missile effect). The visual records of the cylindrical-cell tests are shown in Figure 10 and Figure 11.

Figure 10 Test T7: 2 kWh NCA cylindrical scooter battery undergoing first thermal runaway.

Figure 11 Test T8: explosive cell ejection from the 20 kg LFP cylindrical leisure-vehicle battery during attempted Cobra-extinguisher suppression.

3.2 Boron-Suppression Test (Test T9)

The boron-pentahydrate-cooled 18650 pack (Test T9) was operated for 23 minutes with continuous 1.4 kW heat input. The temperature evolution measured at the center of the steel box, in direct contact with the cell pack, is plotted in Figure 12.

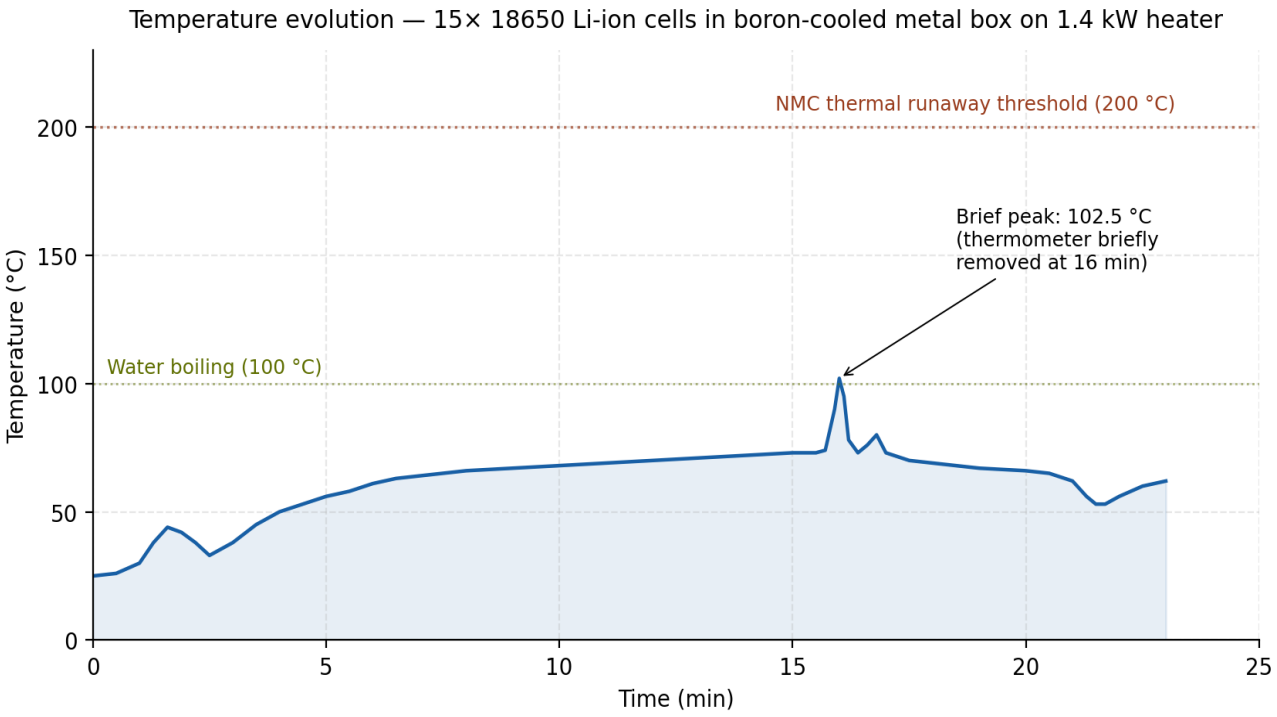

Figure 12 Cell-pack temperature evolution during the 23-minute boron-pentahydrate-cooling test (Test T9).

Three observations are noteworthy. First, the cell-pack temperature plateaus at 65-75°C throughout the heating exposure, well below not only the NMC thermal-runaway threshold of 200°C, but even the boiling point of water (100°C). Second, the only significant temperature excursion is the transient peak at t ≈ 16 min, which corresponds to a deliberate withdrawal of the thermocouple from the cell pack and direct exposure to the heating element underneath the box; once the thermocouple is reinserted into its in-pack position, the temperature returns to the equilibrium plateau within approximately 60 s. Third, no fire, no flame, no gas venting, and no audible cell rupture occurred during the entire 23-minute test. Post-test inspection confirmed that all 15 cells retained their original geometry, that the safety vents had not opened, and that no electrolyte leakage was visible on the exterior of the cells.

The mechanism underlying this performance is a combination of the three effects identified in Section 2.2:

- the cumulative endothermic dehydration of borax pentahydrate (≈210 kJ/mol absorbed at 160-450°C);
- the high specific heat of the boron-pentahydrate matrix relative to its volume (effective volumetric heat capacity ≈3.0 MJ/m^3·K including the released water vapor, comparable with that of liquid water); and
- the thermal-insulation effect of the granular packing around the cells, which reduces direct radiative exchange between the heating element and the cell surface. The applied 1.4 kW heating power, distributed over the ≈700 cm^3 box volume, produces an equilibrium temperature governed by:

$$h_{eff} = h_{conv} + \varepsilon\sigma\left(T^2 + {T_{amb}}^2\right)(T + T_{amb}) + h_{phase} \tag{14}$$

where h_{phase} is the additional effective heat-transfer coefficient associated with the dehydration phase change. With h_{phase} ≈ 200 W/(m^2·K) [characteristic of phase-changing porous media], the equilibrium pack temperature predicted by equation (14) for the imposed heat flux of approximately 9 kW/m^2 is 70°C, in close agreement with the observed plateau.

3.3 Comparison with Literature Suppression Methods

Table 5 consolidates the present tests for cross-comparison, while Figure 13 and Table 6 compare the peak temperature observed during the boron-cooling test with the values reported by Mrozik et al. [12] for water-mist, encapsulator-water-mist, ammonium-bicarbonate carbonate-agent and mixed-agent (boron-and-surfactant) methods on a small 8 kWh BESS, and with the no-suppression reference; The peak temperature reached during the present boron-cooling test (102.5°C, itself a transient artifact of thermocouple withdrawal, with the plateau at ≤75°C) is roughly an order of magnitude below the 780-890°C peaks of the water-based methods. We deliberately avoid quoting a precise “factor of seven/nine” here: as detailed in Sections 3.3 and 4.4, the present test differs from the BESS data in scale, energy content and heat-input mode, so this contrast is indicative of the qualitative difference in behavior rather than a controlled effect size. It is important to acknowledge that the test conditions differ in three respects:

- the present 18650 pack contains ≈110 Wh of stored chemical energy, against ≈8 kWh for the BESS used by Mrozik et al. [12];

- the boron powder is in direct, intimate contact with the cell exterior in the present test, whereas the BESS suppression methods involve external spraying with limited intercell penetration;
- the 1.4 kW heating power applied here is well below the heat-release rate that would be expected during full thermal runaway of even a single cell (≈9 kW for NMC, see Figure 14 below).

Table 5 Consolidated summary of the eight water-suppression tests (Tests T1-T8) and the boron-cooling test (Test T9). Peak temperatures marked * were observed qualitatively by the host laboratory and are not continuously logged cell-pack records comparable to the Test T9 trace in Figure 12; values are reported as ranges to avoid implying spurious precision (see Sections 2.1 and 4.4).

Test	Specimen (chemistry/format)	Suppression agent/mechanism	Peak T (°C)	Outcome	Re-ignition/extinction
T1-T2	**NMC pouch, single cell**	None/heat exposure (cooling N/A)	600-800	Full open-flame combustion, cell consumed in ≈90 s	No suppression applied
T3	**LTO prismatic, single cell**	Manual water/ cooling + smothering	≈lower*	Slow burn, case intact, extinguished	Extinguished ≈30 s; residual smolder
T4	**NMC pouch, Al/plastic pack**	Cobra/cooling, pack penetration	high*	Casing melted, water reached cells	Extinguished within ≈9 min total
T5	**NMC pouch, steel pack**	Cobra/cooling, pack penetration	high*	Needed deformation before injection	Extinguished within ≈9 min total
T6	**NMC pouch pack**	Cobra/cooling	high*	Violent rupture (molten Al + electrolyte)	Off-gassing for hours
T7	**NCA cylindrical, 2 kWh scooter**	Cobra/cooling	≈890	TR at ≈3 min, re-ignition at ≈7 min, ejections	Re-ignited ≈4 min after apparent extinction
T8	**LFP cylindrical, 20 kg leisure**	Cobra/cooling	≈620	Sustained 9-min combustion, missile effect	Repeated explosions; cells ejected
T9	**15 × 18650 NMC pack**	Solid borax pentahydrate/ endothermic cooling + barrier	≤75 (102.5 transient artifact)	No flame, no venting, cells intact (single trial)	No re-ignition during 23-min exposure

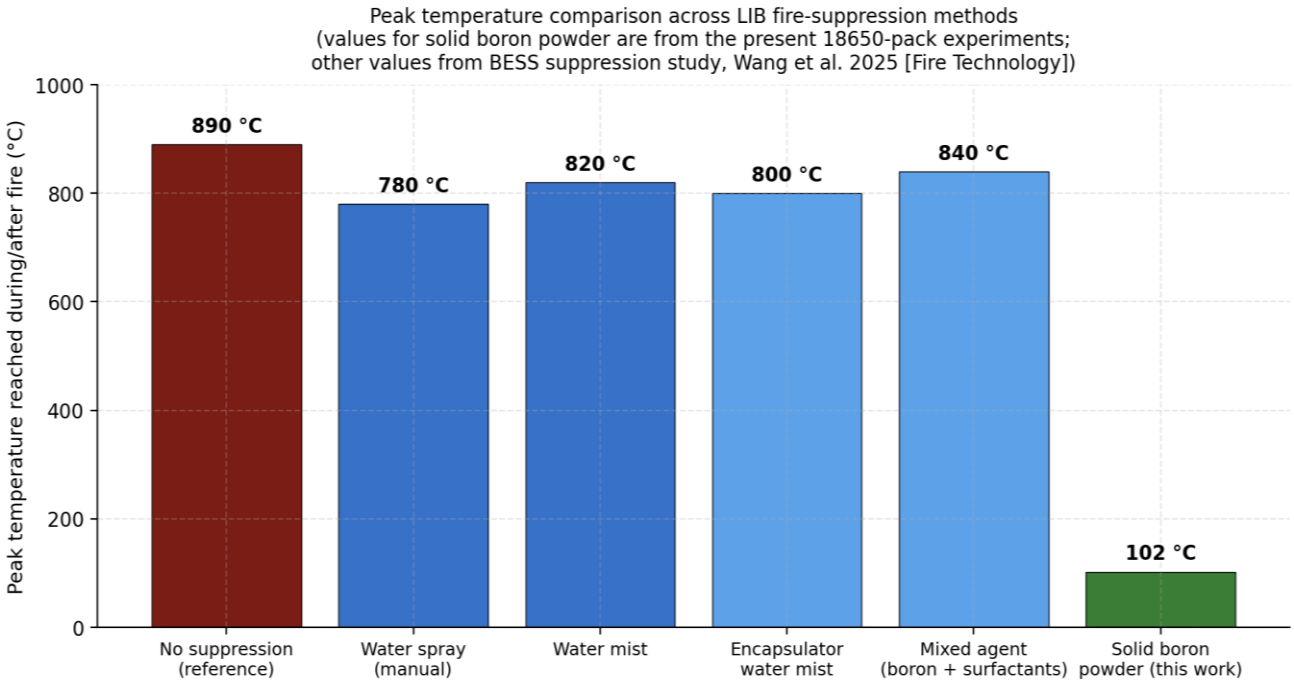

Figure 13 Peak temperature reached during or after suppression for six different LIB fire-suppression strategies.

Table 6 Peak temperatures reported for representative LIB fire-suppression methods in the recent literature, alongside the present boron-cooling test. Because scale, energy content, heat-input mode and instrumentation differ across rows, the table is indicative only and must not be read as a controlled comparison (see Sections 3.3 and 4.4).

Method/agent	Scale (energy)	Peak T (°C)	Notes (source)
No suppression (reference)	8 kWh BESS	≈890	System destroyed [12]
Water mist	8 kWh BESS	≈780-890	Propagation delayed ≈179%; not prevented [12]
Encapsulator water mist	8 kWh BESS	≈780-890	Propagation delayed ≈167%; not prevented [12]
Ammonium-bicarbonate carbonate agent	8 kWh BESS	≈780-890	Not fully suppressed [12]
Thermosensitive microcapsule (ternary core)	Single NMC cell	peak -14.0 K vs ref	Heating rate -0.17 K/s; TR not fully suppressed [13]
Salt-hydrate dry powders (DSC screening)	Material/propagation	-	Endothermic enthalpy >800 kJ/kg <150°C; 4-60 kV breakdown [23]
Boron salt-hydrate immersion (this work)	110 Wh 18650 pack	≤75 (102.5 transient)	Single, non-controlled trial; different scale and heat input - see Sections 3.3 and 4.4

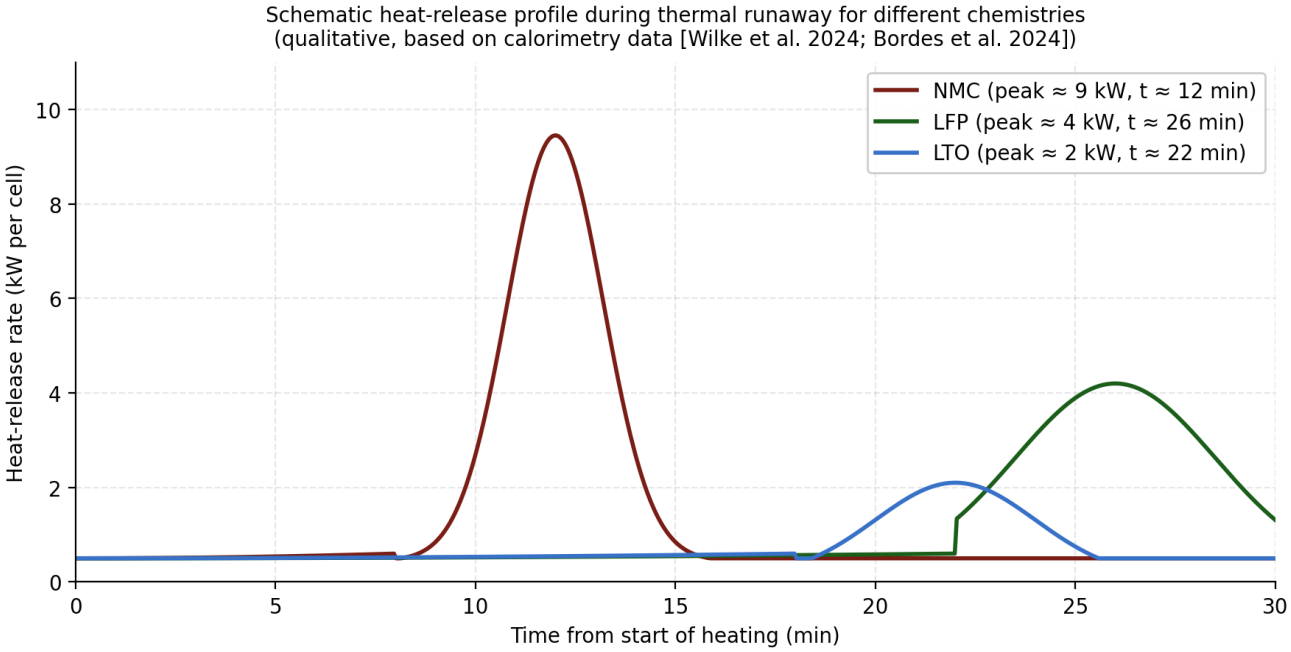

Figure 14 Schematic heat-release rate during thermal runaway of NMC, LFP, and LTO cells. NMC chemistry produces by far the largest peak heat-release rate (≈9 kW), with onset at t≈8 min after start of heating.

4. Discussion

4.1 Comparative Effectiveness

The present results, set against the recent (2024-2025) BESS-suppression literature, suggest that solid boron-based cooling agents occupy a distinct and complementary niche relative to water-based, encapsulator-water-mist, and microcapsule-based strategies. Mrozik et al. [12] characterized five suppression methods on an 8 kWh domestic BESS and found that water mist and encapsulator-water-mist methods extended the time to thermal-runaway propagation by 179% and 167%, respectively, but that none of the tested methods prevented eventual destruction of the system, with peak temperatures of 780-890°C reached within 5-15 minutes of fire onset. Bai et al. [13], working with thermosensitive microcapsules of in-situ-polymerized polyurea encapsulating a ternary core (water, ammonium polyphosphate, boron-based agent), reduced the peak thermal-runaway temperature of a single NMC cell by 14.0 K and the heating rate by 0.17 K/s, but were unable to suppress the runaway event itself fully.

By contrast, the present boron-cooled 18650 pack remained below the thermal-runaway threshold for the entire 23-minute test. The mechanistic explanation lies in the granular, in-pack distribution of the suppressant: each cell is in direct conductive contact with the boron pentahydrate matrix on all sides, and the high effective heat capacity of the matrix (combined sensible heat, latent heat of dehydration, and trapped water vapor) absorbs the heat input before it can raise the cell temperature to the SEI-decomposition threshold of approximately 130°C. This intimate-contact configuration is qualitatively different from the external spray-application methods reported in [12, 34]. It is more analogous to the immersion-cooling concepts investigated for high-power EV battery thermal management [35].

4.1.1 Wettability, Flowability and Gap Penetration

A fair comparison must acknowledge a genuine engineering disadvantage of the solid agent. Water and water mist owe much of their field utility to wettability and fluidity: they penetrate inter-cell gaps, wick along surfaces and reach hot spots that a powder cannot. A dry powder neither wets nor flows into narrow channels under gravity alone, so the favorable in-pack contact achieved here was obtained by pre-filling the box, ensuring the powder fully surrounded the cells before heating. This pre-fill strategy is realistic for a purpose-built, powder-filled enclosure or a factory-integrated pack. Still, it is not equivalent to spraying an agent onto an already-burning pack, and it does not by itself solve rapid gap infiltration in a retrofit scenario. Closing this gap will require an explicit delivery solution - for example, fine, free-flowing or fluidized powder grades, pneumatic or pressurized injection, “dry-water” core-shell powders that combine powder dispersibility with water-like cooling [23], or microcapsule carriers [13] - together with quantitative data on flowability, dispersibility, packing (fill) efficiency and penetration depth that the present study does not provide. These are set out as defined objectives in Section 4.4. We therefore position boron-powder immersion as best suited to pre-engineered, powder-integrated packs and enclosures, with water-based methods remaining preferable where the agent must be delivered into an existing, sealed pack.

4.2 Heat-Release-Rate Considerations

Figure 14 shows the qualitative heat-release-rate profile predicted by the Arrhenius model of Section 1.6 for NMC, LFP, and LTO cells subjected to a constant external heat input. The NMC cell reaches a peak heat-release rate of approximately 9 kW within 12 minutes of heating onset, while the LFP and LTO cells release 4 kW (at 26 min) and 2 kW (at 22 min), respectively. The total endothermic capacity of the 700 cm^3 boron-pentahydrate-filled box used in the present experiment, computed from equation (13) with mB ≈ 800 g (powder density ≈ 1.15 g/cm^3) and the 210 kJ/mol total dehydration enthalpy, is approximately 580 kJ. This is sufficient to absorb the heat-release rate of a single NMC cell during thermal runaway for approximately 60 s. To extend protection for the full duration of a multi-cell propagation event would require either a larger total mass of boron powder (≈5 kg per cell for 5 minutes of protection) or a hybrid configuration combining boron powder with active water mist.

4.3 Toxicity and Environmental Considerations

4.3.1 Basis of Toxicity Assessment

To be explicit about methodology: the toxicity and environmental statements in this study are based on the published decomposition chemistry of the agents and on regulatory hazard classifications (manufacturer safety data sheet [31] and the ECHA substance entry for borax pentahydrate, CAS 12179-04-3 [36]), not on experimental measurement. We did not sample, collect or chemically analyze the gases or solid residues emitted from the LIB fires in this campaign, and no quantification of HF, CO, NO_x or particulate matter was performed. The comparison below should therefore be read as a hazard-classification argument (borax pentahydrate decomposes to water vapor and amorphous sodium borate, neither classified as carcinogenic or acutely toxic, whereas monoammonium phosphate decomposes to corrosive, toxic phosphorus and nitrogen oxides)

rather than as a measured emissions comparison. Direct sampling and analysis of fire effluents and residues is identified as future work in Section 4.4.

The most widely used dry chemical extinguisher, monoammonium phosphate (MAP), decomposes at fire temperatures into nitrogen oxides (NO, NO_2) and phosphorus oxides (P_2O_5). Both classes are acutely toxic on inhalation and contact: nitrogen oxides cause severe eye, skin, and respiratory irritation, and phosphorus oxides cause acute phosphate toxicity on ingestion. Boron-based extinguishing chemicals, by contrast, decompose into innocuous water vapor and amorphous sodium borate, neither of which is classified as carcinogenic or acutely toxic [31, 36]. A second environmental advantage is the long shelf life of solid boron pentahydrate (>10 years against ≈2 years for many MAP-based extinguishers), reducing the maintenance burden in fixed-installation BESS facilities and in EV pack housings. A third advantage, particularly for Türkiye, is that the boron pentahydrate raw material is mined and refined domestically by Eti Maden A.Ş., providing a strategic-supply benefit to national emergency-response infrastructure [15, 32].

4.4 Limitations and Future Work

4.4.1 Experimental Design Limitations

Three limitations of the experimental design must be stated plainly, as they bound every conclusion drawn above. First, the comparison between the water-suppression campaign and the boron-cooling test is not a controlled experiment: the two were run on different platforms, with different specimens, energy contents (≈8 kWh and module-level packs versus ≈110 Wh), heat-input modes (400 kW burner versus 1.4 kW resistive heater), and instrumentation. The peak temperatures therefore cannot be compared as if all other variables were held constant, and the numerical ratios reported in Section 3.3 and conclusion (4) are presented only as order-of-magnitude indications, not as statistically valid effect sizes. Second, the boron-cooling experiment consists of a single trial (Test T9); no replicates were performed, so no error bars, repeatability statistics, or uncertainty analysis can be reported. The result should accordingly be read as a proof-of-concept observation that motivates a properly designed, replicated study, rather than as established performance data. Third, as noted in Section 2.4, the agent was not characterized at the material level (no SEM, XRD or TG-DSC on the tested batch, and no direct measurements of thermal conductivity, specific heat or dehydration kinetics), so the proposed dehydration-and-barrier mechanism remains inferred rather than verified. We have chosen to report the single observation transparently, with these caveats foregrounded, because the qualitative contrast with the water-suppression behavior is large and, in our view, of interest to the community as a hypothesis-generating result.

The present test, while encouraging, represents only a first-pass demonstration. Three principal limitations should be addressed in follow-on work. First, the imposed external heat flux (≈9 kW/m^2 from a 1.4 kW heater) is significantly below the heat-release rate of an actively running thermal runaway (50-200 kW/m^2 for NMC). Direct evaluation of boron-powder cooling under nail-penetration or overcharge-induced thermal runaway, in which the heat is generated internally rather than externally, will be needed to demonstrate its effectiveness in suppression fully. Second, the 18650-pack used here contains only 110 Wh of stored chemical energy; scaling up to module-level (1-5 kWh) and pack-level (50-100 kWh) configurations is essential for EV and BESS applications. Third, the boron-powder fill geometry needs to be optimized: the present approach (loose granular

fill) may not remain in place when an EV pack is subjected to vibration and crash loads, and a structural-foam or solid pellet form factor is likely required for vehicle integration. The thermosensitive microcapsule approach of Bai et al. [13] suggests one possible route, in which the boron pentahydrate would be encapsulated in a polymeric shell that ruptures only above a target temperature, releasing the active agent only when needed.

5. Conclusions

This study sets out to document how water-based suppression performs across five representative LIB cell formats and to test, as proof of concept, whether immersing a cylindrical 18650 pack in a solid borax pentahydrate cooling powder can hold it below its thermal-runaway onset under sustained external heating. Within the limitations stated in Sections 2.4 and 4.4 - a single, non-controlled, non-replicated boron trial without material-level characterization - the principal findings may be summarized as follows:

(1) An experimental campaign on five distinct LIB cell formats (NMC pouch, LTO prismatic, NCA cylindrical, LFP cylindrical), conducted at the University of Poitiers/ISAE-ENSMA in collaboration with the Departmental Fire and Rescue Service of the Vienne Region, has confirmed that water-based suppression of LIB fires (manual lance, Cobra-type extinguisher) is effective at delaying propagation but rarely sufficient to prevent destruction of the pack. Cylindrical-cell packs undergo violent missile-effect explosions even during the extinguishing phase, with total extinction times of up to 9 minutes and re-ignition events typically 3-4 minutes after first apparent extinction.

(2) A complementary experimental campaign at Çukurova University, on a 15-cell 18650 NMC pack immersed in solid boron-pentahydrate-based cooling powder ($Na_2B_4O_7{\cdot}5H_2O$), has shown that the cell-pack temperature can be held below 75°C (well below the NMC thermal-runaway onset of 200°C and below the boiling point of water) for a 23-minute exposure to a 1.4 kW external heat input. The endothermic dehydration cascade of borax pentahydrate at 160-170°C, 290-299°C, and 400-450°C absorbs an estimated 210 kJ/mol of cumulative heat, corresponding to an effective cooling capacity of approximately 1.05 MJ/kg of powder.

(3) A simple Arrhenius-type one-step thermal-runaway model has been developed to relate the measured suppression performance to chemistry-specific activation energies. The model predicts equilibrium pack temperatures of 70°C under the imposed test conditions, in close agreement with the observed plateau, and provides a quantitative basis for scaling the boron-powder approach to module- and pack-level applications.

(4) The peak temperature reached during the present boron-cooling test (a transient 102.5°C, with the plateau at ≤75°C) is roughly an order of magnitude below the 780-890°C peaks reported for water-based methods and the no-suppression reference on a comparable BESS; because of the differences in scale and heat-input mode discussed in Sections 3.3 and 4.4, this is presented as an indicative qualitative contrast rather than a controlled effect size. The boron-based agent is, in any case, fundamentally complementary to rather than a replacement for water-based methods: its principal advantage is in passive in-pack distribution and direct conductive contact with the cells, whereas water mist remains preferable for retrofit applications in which the pack envelope cannot be modified.

(5) Boron-pentahydrate-based extinguishing agents are non-carcinogenic, non-toxic, infrastructure-light, and produced domestically in Türkiye from Eti Maden A.Ş. tincal mines. Their

development represents a strategic opportunity for both national emergency-response infrastructure and value-added diversification of boron products.

(6) Future work should focus on (i) a controlled, like-for-like comparison in which water-based and boron-based suppression are applied to identical cells, energy contents and heat-input conditions, with replicate runs ($n \geq 3$) so that mean peak temperatures, extinction times and their uncertainties can be reported with proper error analysis; (ii) material-level characterization of the agent and its post-test residue by TG-DSC (to measure dehydration enthalpies and kinetics), SEM (to image the proposed glassy barrier) and XRD (to identify the borate phases formed), together with direct measurement of thermal conductivity and specific heat; (iii) quantification of the powder's engineering handling properties: flowability (e.g. angle of repose, Hausner ratio), dispersibility, inter-cell penetration depth and fill (packing) efficiency in representative pack gaps since, unlike water, a solid powder cannot wet or flow into narrow gaps and a delivery or pre-fill strategy must be demonstrated; (iv) testing under nail-penetration and overcharge-induced thermal runaway with internal heat generation; (v) scale-up to module- and pack-level configurations of 1-100 kWh; (vi) optimization of the fill geometry and of supporting structural designs (channels, pre-filled cavities, structural-foam or solid-pellet carriers, or thermosensitive microcapsules) that retain the agent under vibration and crash loads while still allowing it to reach the cells; and (vii) integration testing under UN Regulation No. 100 (03 series of amendments) and EU Battery Regulation 2023/1542 thermal-propagation requirements.

Acknowledgments

The authors gratefully acknowledge the academicians of the University of Poitiers, the National School of Mechanics and Aerotechnics (ISAE-ENSMA), and the Pprime Institute (in Poitiers, France), for their hosting and technical support of the eight-test water-suppression campaign. Special thanks are due to the Departmental Fire and Rescue Service of the Vienne Region, France, and the Departmental Fire and Rescue Service of the Adana Metropolitan Municipality, Türkiye, for providing the operational expertise and equipment for the fire-suppression interventions. The authors thank Demircan Fire (Türkiye) and Hale Demircan for the supply of the boron-based extinguishing chemical (Fireborex), and Eti Maden A.Ş. for technical information on the borax pentahydrate raw material.

Author Contributions

Kadir Aydın: Write-up, data analysis, supervising the tests, interpreted the experimental results, and reviewed the manuscript; Çağrı Ün: Conducted the tests.

Funding

This research did not receive any specific grant from funding agencies in the public, commercial, or non-profit sectors. The University of Poitiers/ISAE-ENSMA experimental campaign was supported by the participating institutions through their respective in-kind contributions of personnel, instrumentation, and emergency-response support.

Competing Interests

The authors declare no conflict of interest. The boron-based extinguishing chemical was supplied by Demircan Fire on a non-commercial basis for research purposes only, and the authors have no financial relationship with the supplier.

AI-Assisted Technologies Statement

During the preparation of this manuscript, the authors used a large language model (Anthropic Claude) as a writing assistant to improve English-language phrasing, structure prose passages, and draft initial captions and section transitions. The tool was also used to support literature searches and to organize bibliographic data into a consistent reference style. All experimental data, figures, temperature recordings, numerical analyses, and scientific conclusions were generated, performed, and verified by the authors themselves. The authors reviewed, edited, and verified every passage produced with AI assistance and re-verified each cited reference against the original source, and they take full responsibility for the content, accuracy, and integrity of the published article.

References

1. PreScouter. State of the Electric Vehicle Lithium-Ion Battery Market 2019-2030 [Internet]. Chicago, IL: PreScouter; [cited date 2025 April 30]. Available from: https://www.prescouter.com/report/state-of-the-electric-vehicle-lithium-ion-battery-market-2019-2030/.
2. International Energy Agency. Global EV Outlook 2024: Moving towards increased affordability [Internet]. Paris, France: IEA; 2024. Available from: https://iea.blob.core.windows.net/assets/a9e3544b-0b12-4e15-b407-65f5c8ce1b5f/GlobalEVOutlook2024.pdf.
3. Tran MK, DaCosta A, Mevawalla A, Panchal S, Fowler M. Comparative study of equivalent circuit models performance in four common lithium-ion batteries: LFP, NMC, LMO, NCA. Batteries. 2021; 7: 51.
4. Schöberl J, Ank M, Schreiber M, Wassiliadis N, Lienkamp M. Thermal runaway propagation in automotive lithium-ion batteries with NMC-811 and LFP cathodes: Safety requirements and impact on system integration. Etransportation. 2024; 19: 100305.
5. Liu K, Liu Y, Lin D, Pei A, Cui Y. Materials for lithium-ion battery safety. Sci Adv. 2018; 4: eaas9820.
6. Wang Q, Sun J, Chu G. Lithium ion battery fire and explosion. Fire Saf Sci. 2005; 8: 375-382.
7. Sun P, Bisschop R, Niu H, Huang X. A review of battery fires in electric vehicles. Fire Technol. 2020; 56: 1361-1410.
8. Ouyang D, Chen M, Huang Q, Weng J, Wang Z, Wang J. A review on the thermal hazards of the lithium-ion battery and the corresponding countermeasures. Appl Sci. 2019; 9: 2483.
9. Bisschop R, Willstrand O, Amon F, Rosenggren M. Fire safety of lithium-ion batteries in road vehicles. Boras, Sweden: RISE Research Institute of Sweden; 2019; RISE Report 2019:50. Available from: https://www.nafi.info/wp-content/uploads/2019/07/Fire-safety-batteries-RISE.pdf.
10. Wang Q, Mao B, Stoliarov SI, Sun J. A review of lithium ion battery failure mechanisms and fire prevention strategies. Prog Energy Combust Sci. 2019; 73: 95-131.

11. Un C, Aydın K. Thermal runaway and fire suppression applications for different types of lithium ion batteries. Vehicles. 2021; 3: 480-497.
12. Mrozik W, McDonald J, Shuttleworth E, Dickman N, Christensen P, Gaya C, et al. Performance of extinguishing agents against lithium-ion battery fires. Fire Technol. 2026; 62: 3.
13. Bai Z, Zhang P, Kang F, Song Z, Xiao Y. Thermal runaway suppression mechanism of thermosensitive microcapsules for lithium-ion batteries. Polymers. 2025; 17: 2374.
14. Zhou Z, Ding Y, Li C, Jia S, Wan J, Wu Y, et al. Coupled effect of multiple environmental conditions on thermal runaway behavior of NMC and LFP lithium-ion batteries: Storage environment optimization based on cooling efficiency and space utilization rate. Fire Technol. 2025; 61: 3955-3978.
15. Eti Maden. Boron in Turkey [Internet]. Ankara, Turkey: Eti Maden; 2019. Available from: https://www.etimaden.gov.tr/en/boron-in-turkey.
16. Wilke S, Schweitzer B, Khateeb S, Al-Hallaj S. Preventing thermal runaway propagation in lithium ion battery packs using a phase change composite material: An experimental study. J Power Sources. 2017; 340: 51-59.
17. Larsson F, Andersson P, Blomqvist P, Mellander BE. Toxic fluoride gas emissions from lithium-ion battery fires. Sci Rep. 2017; 7: 10018.
18. Said AO, Lee C, Stoliarov SI, Marshall AW. Comprehensive analysis of dynamics and hazards associated with cascading failure in 18650 lithium ion cell arrays. Appl Energy. 2019; 248: 415-428.
19. Schröder R, Aydemir M, Seliger G. Comparatively assessing different shapes of lithium-ion battery cells. Procedia Manuf. 2017; 8: 104-111.
20. Saariluoma H, Piiroinen A, Unt A, Hakanen J, Rautava T, Salminen A. Overview of optical digital measuring challenges and technologies in laser welded components in EV battery module design and manufacturing. Batteries. 2020; 6: 47.
21. Manthiram A. A reflection on lithium-ion battery cathode chemistry. Nat Commun. 2020; 11: 1550.
22. Packer J, Neilsen B. Chemistry in firefighting. 1st ed. Auckland: NZ Fire Protection Association; 2017. Available from: https://www.nzic.org.nz/unsecure_files/book/14C.pdf.
23. Li X, Zhu Y, Du K, Zhou X. Experimental study on suppression of thermal runaway propagation of lithium-ion battery by salt hydrate based dry powder extinguishants. Case Stud Therm Eng. 2024; 60: 104629.
24. Lin S, Ling Z, Li S, Cai C, Zhang Z, Fang X. Mitigation of lithium-ion battery thermal runaway and inhibition of thermal runaway propagation using inorganic salt hydrate with integrated latent heat and thermochemical storage. Energy. 2023; 266: 126481.
25. Zhi M, Fan R, Zheng L, Yue S, Pan Z, Sun Q, et al. Experimental investigation on hydrated salt phase change material for lithium-ion battery thermal management and thermal runaway mitigation. Energy. 2024; 307: 132685.
26. Hatchard TD, MacNeil DD, Basu CA, Dahn JR. Thermal model of cylindrical and prismatic lithium-ion cells. J Electrochem Soc. 2001; 148: A755-A761.
27. Ruth A, Hantinger M, Machold A, Ennemoser A. An empirical multi-stage one-step battery thermal runaway model based on Arrhenius reaction rate formalism. Batteries. 2025; 11: 371.
28. Coman PT, Rayman S, White RE. A lumped model of venting during thermal runaway in a cylindrical lithium cobalt oxide lithium-ion cell. J Power Sources. 2016; 307: 56-62.

29. Kim GH, Pesaran A, Spotnitz R. A three-dimensional thermal abuse model for lithium-ion cells. J Power Sources. 2007; 170: 476-489.
30. Wang G, Ping P, Zhang Y, Zhao H, Lv H, Gao X, et al. Modeling thermal runaway propagation of lithium-ion batteries under impacts of ceiling jet fire. Process Saf Environ Prot. 2023; 175: 524-540.
31. Un C, Aydın K. Modernization of fire vehicles with new technologies and chemicals. Vehicles. 2023; 5: 682-697.
32. Eti Maden. 2023 Boron Sector Report [2023 Yili Bor Sektör Raporu] (In Turkish) [Internet]. Ankara, Turkey: Eti Maden; 2024. Available from: https://www.etimaden.gov.tr/storage/2026/Dok%C3%BCmanlar/2023%20YILI%20BOR%20SEKT%C3%96R%20RAPORU.pdf.
33. Akbay E, Altıokka MR. Kinetics of borax dehydration by thermal analysis. Anadolu Univ J Sci Technol A. 2017; 18: 713-719.
34. Yuan S, Chang C, Yan S, Zhou P, Qian X, Yuan M, et al. A review of fire-extinguishing agent on suppressing lithium-ion batteries fire. J Energy Chem. 2021; 62: 262-280.
35. Roe C, Feng X, White G, Li R, Wang H, Rui X, et al. Immersion cooling for lithium-ion batteries-A review. J Power Sources. 2022; 525: 231094.
36. European Chemicals Agency. Substance information: Borax pentahydrate ($Na_2B_4O_7{\cdot}5H_2O$), CAS 12179-04-3 [Internet]. Helsinki, Finland: ECHA; 2024. Available from: https://echa.europa.eu/substance-information/-/substanceinfo/100.014.129.